

Suresh, A.  
Space Science  
Modeling Sharp Jumps in Flux Tube Entropy in the Earth's Magnetosphere

Modeling Sharp Jumps in Flux Tube Entropy in the Earth's Magnetosphere

Anirudh Suresh

Space Science

St. John's School, Houston, TX

## Abstract

This study seeks to understand the quiet auroral arcs that appear in the evening sky at high latitudes. Due to the lack of methods that reliably predict these arcs' configurations, this research aimed to calculate the plasma and magnetic signatures in cases of arc-forming and non-arc-forming jumps in plasma parameters through a novel computational model based on integration of differential equations. The model computes the magnetic field for various computer-simulation experimental scenarios by calculating the position, pressure, and magnetic field strength at points along each magnetic field line. Tests were performed to check that the equations were solved correctly. The model predicts that arc-forming and non-arc-forming jumps imply a sharp decrease in equatorial field strength in the plasma sheet region of the magnetosphere. A planned future study aims to analyze magnetospheric spacecraft data to search for the kinds of signatures this model predicts; if it successfully locates those signatures, it will have confirmed the driving force behind auroral arc formation. Another direction for follow-up research is the study of the association between arc-forming or non-arc-forming jumps and magnetospheric substorms, electromagnetic and particle disturbances in the plasma sheet and ionosphere that can disrupt spacecraft operations and damage power systems on Earth.

## Introduction

The Earth's magnetosphere is the region of space in which the Earth's magnetic field has primary control over the motion of charged particles. The magnetic field of the magnetosphere is not the Earth's generic dipole but rather a rounded structure on the dayside (facing the Sun) and a stretched tail-like shape (the magnetotail) on the nightside. This stretched shape is a result of the solar wind, ionized plasma (mostly in the form of  $H^+$ ,  $He^{2+}$ , and  $e^-$ ) streaming away from the Sun; solar wind ions move at such a high speed that they draw the nightside magnetosphere out into a long tail that extends beyond lunar orbit [Baumjohann and Treumann, 1996].

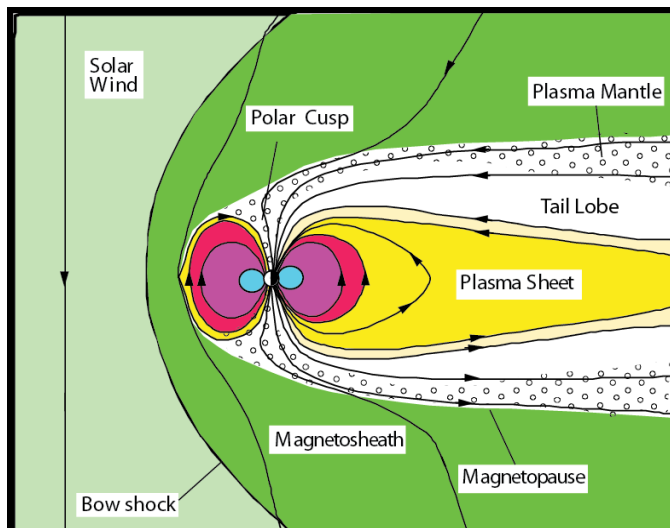


Figure 1. A cartoon representation of the magnetosphere [Wolf, 2015].

The magnetosphere consists of various regions and structures, many of which are shown in Figure 1 to the left. This study focuses on the plasma sheet, which contains a sheet of electrical current that flows westward across the tail. The plasma sheet is the primary source of the particles that cause magnetic storms, the aurorae, and most magnetospheric dynamics.

Charged particles move much more easily along the magnetic field than perpendicular to it, so the magnetic field constrains the particle distribution [Baumjohann and Treumann, 1996].

The primary electromagnetic and particle disturbance in the plasma sheet is known as the magnetospheric substorm and takes place due to the plasma sheet's weak magnetic field. The field is weakest where it switches from earthward to tailward, which is always near the center of the current sheet in stretched configurations. Under normal circumstances, when the amount of

Modeling Sharp Jumps in Flux Tube Entropy in the Earth's Magnetosphere  
plasma in the region is below a certain threshold, the cross-tail current sheet is thick enough to carry the electrical current, and the plasma is approximately frozen to the magnetic field. These conditions conserve the flux tube entropy  $PV^\gamma$ , where  $\gamma$  is the adiabatic constant  $5/3$ ,  $P$  is particle pressure, and  $V$  is the volume of a bundle of flux tubes (regions in space that have a magnetic field) containing one unit of magnetic flux. However, during the growth phase of the substorm, plasma energy gradually builds up in the plasma sheet. As a result, the magnetic field lines gradually change from a rounded, dipolar shape into a more stretched configuration, and the current sheet becomes too thin to carry the required current. When this occurs, the plasma unlocks from the magnetic field, ushering in the expansion phase of the substorm. Down-flowing electrons move into the upper ionosphere in high-latitude regions of the Earth and cause dramatic brightening of the aurorae. The sudden brightening of the most equatorward auroral arc in the evening sky defines the onset of the expansion phase [*Baumjohann and Treumann, 1996*].

Meanwhile, plasma sheet field lines that acquired a stretched shape during the growth phase collapse back to a dipolar configuration in the expansion phase. The field lines pinch off from themselves in a process called reconnection in which magnetic field energy is converted into thermal and kinetic energy, forming a set of dipolar field lines closer to Earth and another set of field lines unconnected to the Earth. Through this process, magnetic energy is released, and plasma is injected into the geosynchronous-orbit region of the equatorial plane. Electrons also flow into the ionosphere to form bright aurorae. Finally, by the recovery phase, the energy release and auroral brightening have gradually come to a close, and the plasma sheet returns to a state mostly similar to that at the onset of the growth phase [*Baumjohann and Treumann, 1996*].

As of now, a fundamental understanding of the substorm exists, but specialized knowledge of the mechanism behind the onset of the expansion phase, particularly with respect

Modeling Sharp Jumps in Flux Tube Entropy in the Earth's Magnetosphere to what triggers it, is lacking. Specifically, there is no conventionally accepted theory of the magnetospheric structures associated with the quiet evening auroral arcs, including those that suddenly brighten and break up at the beginning of the substorm expansion phase. Though there are computational models that represent features of plasma sheet dynamics during substorms (e.g. *Birn and Hesse*, 1991; *Raeder et al.*, 2010; *Pritchett and Coroniti*, 2011; *Sitnov and Swisdak*, 2011), none have the ability to couple to the ionosphere on a scale as fine as an auroral arc, which is typically 0.1 to 10 km thick [Borovsky, 1993]. The relationship between magnetospheric parameters and the field-aligned current is given by an equation derived by *Vasyliunas* [1970], which is presented in (1).  $J_{\parallel}$  is the density of the field-aligned electrical current into the ionosphere, and  $\hat{b}$  is the direction of the magnetic field. (1) suggests that a sharp jump in  $PV^{\gamma}$  generates a thin, intense sheet of field-aligned current. If the current is upward, it is carried by downward-moving electrons and thus corresponds to the formation of an auroral arc. Sharp jumps that generate downward currents do not correspond to arc formation.

$$J_{\parallel} = \frac{1}{2} \hat{b} \cdot \nabla V \times \nabla P = \frac{\hat{b} \cdot \nabla V \times \nabla PV^{\gamma}}{2V^{\gamma}} \quad (1)$$

This study focused on creating a 2D computational model of sharp jumps in  $PV^{\gamma}$  in the plasma sheet. This model uses an xz-coordinate system in which x refers to distance from the Earth in the direction away from the Sun (along the Sun-Earth axis) and z refers to distance north. Having an accurate model of plasma sheet properties will allow for better understanding of the substorm. Moreover, such a model could clarify the process behind substorm expansion by allowing for further computer-simulation experiments and studies of substorm onset.

Furthermore, part of the rationale for creating such a model derives from the effects of plasma on spacecraft. Often, the electrons from the plasma sheet can accumulate on protrusions

Modeling Sharp Jumps in Flux Tube Entropy in the Earth's Magnetosphere of a spacecraft, such as antennae. This problem is especially severe during the substorm expansion phase, when electrons stream toward Earth and penetrate to geosynchronous orbit, home to hundreds of operating spacecraft. When this happens, the differential charging of different parts of the spacecraft can cause sparks to jump around the craft, wreaking havoc on the spacecraft's circuits. Implementing solutions to such a problem can be expensive and laborious; frequently, for instance, the spacecraft has to be rebooted, which entails many hours out of operation [Lanzerotti, 2001]. Having concrete data pertaining to the configuration of the plasma in critical regions of the magnetosphere could allow for the prediction and prevention of a dilemma in which the capabilities of a spacecraft near the plasma sheet are disabled.

Another area of interest is geomagnetic storms, large disturbances in Earth's magnetic field caused typically by either solar coronal mass ejections (CMEs), in which immense amounts of plasma are released by the Sun toward Earth, or high-speed solar wind streams. During a geomagnetic storm, several powerful accompanying substorms typically hit the Earth and alter the magnetic field strength on Earth, each on a time scale of about one minute. According to Faraday's Law, when  $\partial \mathbf{B} / \partial t$ , the rate of change of magnetic field, gets large, the magnitude of the curl of the electric field increases proportionally. Therefore, if an immense amount of plasma were to reach the Earth, the magnetic field would intensify rapidly, and an unhealthy amount of electricity would flow through the power system and melt transformers and wires.

This destructive potential of the greatest geomagnetic storms is well-documented: in 1859, a powerful CME storm disrupted the global telegraph system, setting wires and offices on fire. And in July 2012, a CME storm of similar magnitude burst past a spacecraft that was on the opposite side of the Sun. If the Earth had happened to be in the path of that CME, that storm would have caused extensive damages to the power grid, satellite transmissions, and

Modeling Sharp Jumps in Flux Tube Entropy in the Earth's Magnetosphere telecommunications. The National Academy of Sciences estimates that resulting power outages could last months to years and that the cost in damages could exceed two trillion dollars [Phillips, 2014]. As a result, finding a way to predict, study, and eventually solve this problem by first understanding the magnetic signature of the substorm is of interest, for it could potentially facilitate efforts to resolve the dangers of geomagnetic storms and substorms.

## The Method behind the Model

*Griffiths* [1981] shows the relationship between the magnetic field  $\mathbf{B}$  and the vector potential  $\mathbf{A}$ .

$$\mathbf{B} = \nabla \times \mathbf{A} \quad (2)$$

When  $\mathbf{B}$  is assumed to be in the xz-plane, we can choose  $\mathbf{A} = A(x, z)\hat{\mathbf{y}}$  so that

$$\mathbf{B} = \nabla A \times \hat{\mathbf{y}} \quad (3)$$

$A$  is constant along a magnetic field line, so it can be easily used as a label for the field lines. The Maxwell equation for magnetic force and current in the magnetosphere is [*Griffiths*, 1981]

$$\nabla \times \mathbf{B} = \mu_0 \mathbf{J} \quad (4)$$

where  $\mathbf{J}$  is the current density and  $\mu_0$  is the constant known as the vacuum permeability and is equal to  $400\pi (\text{nT})^2/\text{nPa}$ , where the nT (nanotesla) is a unit of magnetic field strength and the nPa (nanopascal) is a unit of pressure. The equation of magnetic equilibrium is [*Dendy*, 1993]

$$\nabla P = \mathbf{J} \times \mathbf{B} \quad (5)$$

where  $P$  is the particle pressure. This relationship causes the pressure gradient to balance the magnetic force. Since  $\mathbf{J} \times \mathbf{B}$  is orthogonal to  $\mathbf{B}$ , the dot product of  $\mathbf{J} \times \mathbf{B}$  and  $\mathbf{B}$  is 0. (5) implies  $\nabla P \cdot \mathbf{B} = 0$ . Hence, pressure is constant along a field line. It is thus a function of field line index, or  $A$ , and can be expressed as  $P(A)$ . Substituting in (3) and (4), (5) can be written as

$$\frac{dP}{dA} \nabla A = \frac{1}{\mu_0} \{ \nabla \times (\nabla A \times \hat{y}) \} \times (\nabla A \times \hat{y}) = -\frac{1}{\mu_0} \nabla^2 A \cdot \nabla A \quad (6)$$

which produces the Grad-Shafranov partial differential equation [*Fuchs and Voigt, 1979*]

$$\nabla^2 A = -\mu_0 \frac{dP}{dA} \quad (7)$$

This 2D partial differential equation has often been used to compute magnetospheric equilibria (for instance, *Hau et al [1989]*). The model created in this study implements a different procedure that stems from rewriting (5) using (4). The rewritten form is given in (8).

$$\nabla P = \frac{\nabla \times \mathbf{B}}{\mu_0} \times \mathbf{B} = -\nabla \left( \frac{B^2}{2\mu_0} \right) + \frac{(\mathbf{B} \cdot \nabla) \mathbf{B}}{\mu_0} \quad (8)$$

$$\frac{\partial B}{\partial A} = -\frac{\mu_0}{B} \frac{dp}{dA} + \frac{\boldsymbol{\kappa} \cdot \nabla A}{B} \quad (9)$$

$$\frac{dp}{dA} = \frac{\frac{1}{V^\gamma} \frac{d(PV^\gamma)}{dA} + 2\gamma p <\frac{\boldsymbol{\kappa}}{B}> + \frac{2\gamma p B_{zb}}{VB_b^2 |B_{xb}|}}{1 + \frac{\gamma <\beta>}{2}} \quad (10)$$

This study's model solves (9) and (10), differential equations derived from Maxwell's equations under force equilibrium. (9), the force-balance condition, comes directly from (8), and (10) is based on (9) and geometrical considerations.  $\boldsymbol{\kappa}$  is the curvature vector, and  $B_{zb}$ ,  $B_{xb}$ , and  $B_b$  refer to the z-component, x-component, and magnitude, respectively, of the magnetic field at the near-Earth boundary. The brackets indicate the average of a value over a flux tube.

The vast majority of this research was done through computer programming in Wolfram Mathematica and MATLAB. The procedure for the first step has a logically derived order: first, an analytic expression for  $A$  is used to calculate a number of x- and z-points along the proposed first field line, equally spacing those points along the field line. The analytic expressions for  $A$  and  $P$  are given by either (11) or (12), depending on the case being considered.

$$A(x, z) = -A_0 \cos\left(\frac{\pi z}{2\Delta}\right) e^{-\frac{\pi x}{2\Delta}} \quad P(x, z) = 0 \quad (11)$$

$$A(x, z) = -A_0 \cos\left(\frac{\pi z}{2\Delta}\right) e^{-\alpha x} \quad P(x, z) = \frac{1}{2\mu_0} \left[ \left(\frac{\pi}{2\Delta}\right)^2 - \alpha^2 \right] A(x, z)^2 \quad (12)$$

(11) and (12) constitute exact analytic solutions to (7). (11) and (12) apply to  $A \leq a_1$  (red curve and to the left in Figure 2), while the model computes field lines for  $A \geq a_1$  (red curve and to the right in Figure 2). So, (11) and (12) present the initial boundary conditions to the model. In (12),  $\alpha$  equals  $0.1 R_E$ , where  $R_E$  represents a length equivalent to the radius of the Earth.  $\Delta$  equals  $5.23598 R_E$  in (11) and  $2 R_E$  in (12), and  $A_0$  equals  $2075.50 \text{ nT } R_E$  in (11) and  $100 \text{ nT } R_E$  in (12). The next step is to calculate  $\hat{b}$ , the unit direction vector of the magnetic field, and  $\kappa$  through a variable spacing five-point difference equation adapted from *Singh and Bhadauria [2009]*. The variable spacing procedure is necessary because, moving from field line to field line, the spacing becomes skewed with points moving away from  $z = 0$ , the equatorial plane (the x-axis), toward  $x = 0$ , the near-Earth boundary (the z-axis).  $\hat{b}$  uses the x- and z- values in the difference equation, while  $\kappa = (\hat{b} \cdot \nabla)\hat{b}$ . Then, the gradient of the analytic expression in (11) or (12) is taken in order to get  $\mathbf{B}$ , the magnetic field.  $\mathbf{B}$  is in the same direction as  $\hat{b}$  but with the actual magnitude of the magnetic field at each point along the field line.

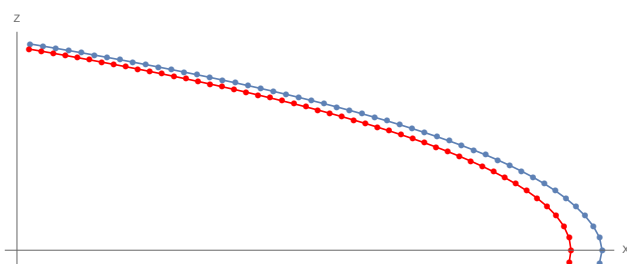


Figure 2. Visualization of step-up method. The red curve represents field line 1 with  $A = a_1$ , and the blue curve is field line 2 with  $A = a_1 + \Delta A$ . Field line 2 is computed from field line 1 and is then used to compute the next field line.

Next is the actual step-up from the first field line to the second. This model utilizes small steps in  $A$  in order to use a first-order step-up method. To the left, Figure 2 gives a general idea of the model's step-up method. The red

This step-up involves first calculating the position of the second field line from the

position and magnetic field strength of the first field line through (13).

$$\mathbf{S}_k(A + \Delta A) = \mathbf{S}_k(A) + \frac{\Delta A}{B_k(A)} \left\{ \frac{[x_{k+1}(A) - x_{k-1}(A)] \hat{z} - [z_{k+1}(A) - z_{k-1}(A)] \hat{x}}{\sqrt{[x_{k+1}(A) - x_{k-1}(A)]^2 - [z_{k+1}(A) - z_{k-1}(A)]^2}} \right\} \quad (13)$$

$\mathbf{S}_k$  refers to the vectorized position  $\{x, z\}$  at point  $k$  along the field line whose  $A$  value is designated in parenthesis. The subscript serves as the index for the points along a field line, and  $\hat{x}$  and  $\hat{z}$  are unit vectors in the x- and z-directions, respectively. (13) essentially steps from field line 1 to field line 2 by moving each point a distance of  $\Delta A/B_k(A)$  perpendicular to field line 1.

Then, the jump in  $PV^\gamma$  is computed using an analytic expression given by (14).  $dPV^\gamma/dA$ , the change in  $PV^\gamma$  with respect to change in  $A$ , is subsequently used to calculate  $dP/dA$  in (10), which is then utilized in (9) to compute  $dB/dA$ , yielding the next set of B magnitudes.

$$\frac{dPV^\gamma}{dA} = \begin{cases} \frac{\pi \Delta PV^\gamma}{2A_w} \sin\left(\frac{A - A_{\min}}{A_w} \pi\right) & \text{if } A_{\min} \leq A \leq A_{\min} + A_w \\ 0 & \text{elsewhere} \end{cases} \quad (14)$$

(14) is a peak function manually created with width  $A_w$  and area  $\Delta PV^\gamma$ . It is sharply peaked at  $A_{\min} + 0.5 A_w$ .  $A_{\min}$  is the  $A$ -value of the field line at which the jump in  $PV^\gamma$  begins.  $\Delta PV^\gamma$ , measured in nPa ( $R_E/nT$ ) $^\gamma$ , refers to the magnitude of the jump, and  $A_w$ , the range over which that jump occurs, is proportional to arc width in cases of auroral arc formation.

This step-up process from (13) to (14) and (9) to (10) is the backbone of the program and is repeated to move from field line  $n$  to field line  $n+1$ . For field lines after the first, an analytic expression for  $\mathbf{B}$  does not exist, so separate  $\hat{b}$  unit vectors and B magnitude values will be calculated and multiplied for each point to obtain the complete  $\mathbf{B}$  vector. Moreover, as more field lines are computed, the originally equal spacing between points deteriorates. To preserve

Modeling Sharp Jumps in Flux Tube Entropy in the Earth's Magnetosphere resolution near the equatorial plane, the region for which detailed understanding is key, a dense accumulation of points is needed. As a result, a four-point interpolation scheme adapted from *Singh and Bhadauria* [2009] equally re-spaces the points. Its ability to provide access to more detail in the critical region outweighs the slight inaccuracy it produces in recreating field lines.

## Results

This study focuses on computer-simulation experimental scenarios with sharp jumps in  $PV^\gamma$  at the inner edge of the plasma sheet based on (11) that generate downward current (no arc formation) and those embedded within the plasma sheet based on (12) that generate upward current (arc formation). In these, a mathematical instability often limits the range of field lines the program can compute. This instability is linked to the method's boundary conditions and differs from numerical instabilities, which can usually be ameliorated by adjusting grid spacing or other parameters. In the next section, entitled "Accuracy," this instability is discussed further.

In each experimental scenario, key input parameters are shifted to change the configuration of the field lines. Several different combinations of  $\Delta PV^\gamma$  and  $A_w$  with jumps located both at the inner edge of the plasma sheet and embedded within the plasma sheet were considered in the study. The table below designates the different scenarios studied.

Scenario Name	Location of Jump	$\Delta PV^\gamma$ (nPa ( $R_E/nT$ ) $^\gamma$ )	$A_w$ (nT $R_E$ )
1A	Inner edge	0.10	1
2A	Inner edge	0.47	1
1B	Embedded	0.05	0.1
2B	Embedded	0.10	0.1

An  $A_w$  value of 1 nT  $R_E$  in the inner edge case is consistent with an arc thickness of a few km. Yet arc thicknesses vary from 100 m to 10 km [*Borovsky*, 1993]. In the case of embedded

Modeling Sharp Jumps in Flux Tube Entropy in the Earth's Magnetosphere  
arcs,  $A_w = 0.1 \text{ nT } R_E$  was chosen to minimize the instability's effect.  $\Delta PV^\gamma = 0.47 \text{ nPa } (R_E/\text{nT})^\gamma$

represents an average observed value in the middle plasma sheet [Xing and Wolf, 2007].

In case A, jumps in  $PV^\gamma$  were found to produce a trend of magnetic field configurations. Figures 3-5 show results for 1A. In the Figures, the axes labeled "X" and "Z" have units of  $R_E$ . The field lines become more stretched as the jump takes place, but the effect is not dramatic. The more telling signs of the jump include substantially more spacing between field lines equally distanced in  $A$  and the decrease in the magnetic field along the equatorial plane.

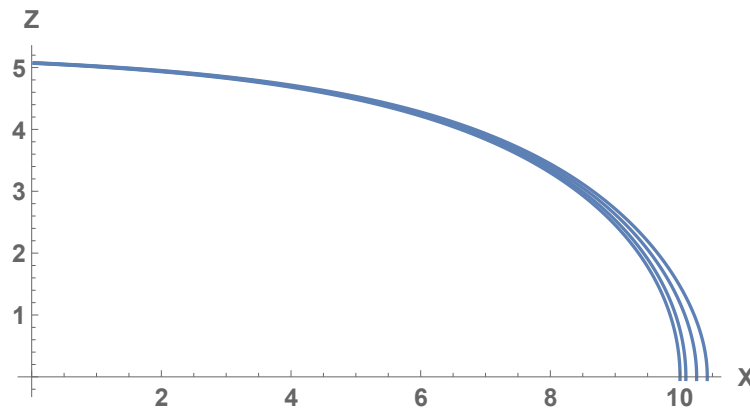


Figure 3. A plot of 4 field lines in 1A, with the field lines shown spaced equally in  $A$  (2.055 nT  $R_E$ ). Note the increased spacing between the field lines near the equatorial plane.

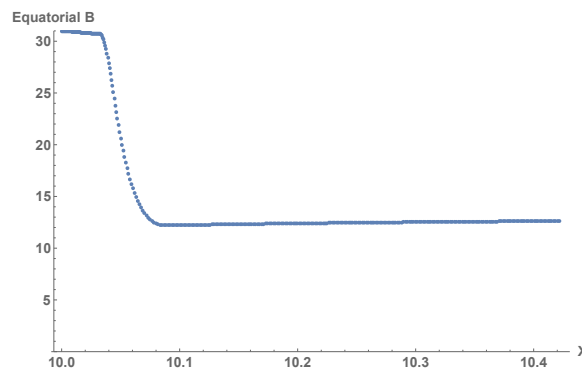


Figure 4. A plot of magnetic field strength (nT) along the equatorial plane in 1A.

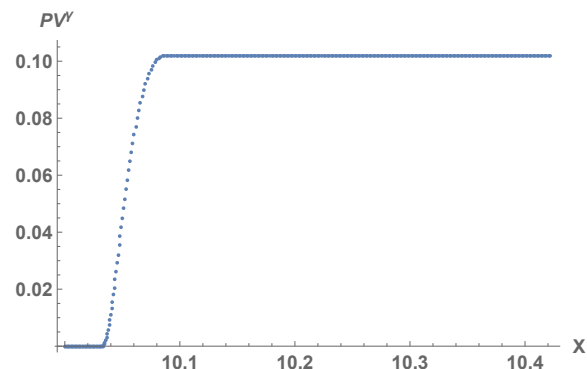


Figure 5. A plot of  $PV^\gamma$  (nPa  $(R_E/\text{nT})^\gamma$ ) along the equatorial plane in 1A.

Figures 6-8 show results for case 2A. Increasing distance between field lines separated equally in  $A$  (Figure 6) indicates weakening magnetic field (Figure 7). In 2A, not only does the spacing between field lines increase; the shape of the field line itself is dramatically altered. As

Modeling Sharp Jumps in Flux Tube Entropy in the Earth's Magnetosphere  
the jump in  $PV^\gamma$  progresses, an increasingly sharp protrusion centered on the equatorial plane

develops. This "knob" in the field line is defined by change in the curvature close to the equatorial plane (from negative to positive to negative) and accompanies a dramatic shift in  $PV^\gamma$  (Figure 8). Additionally, the decrease in equatorial magnetic field strength is more intense than in 1A; while in 1A the magnetic field strength reaches a minimum of around 12.2 nT from an original value of 31 nT, in 2A it descends to a deep minimum of 0.874 nT, a very potent indication of a large jump in  $PV^\gamma$ . Furthermore, in both 1A and 2A, the jump in  $PV^\gamma$  causes a high current density perpendicular to the field lines in the equatorial plane.

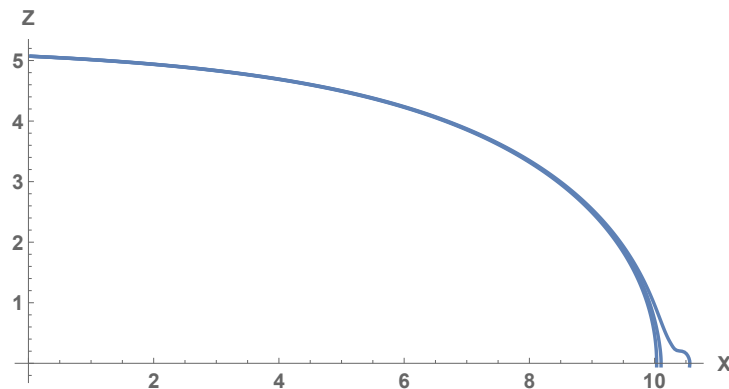


Figure 6. A plot of 4 field lines in 2A, with the field lines shown spaced equally in  $A$  ( $0.487$  nT  $R_E$ ). Note the increased spacing between the field lines and the formation of a knob.

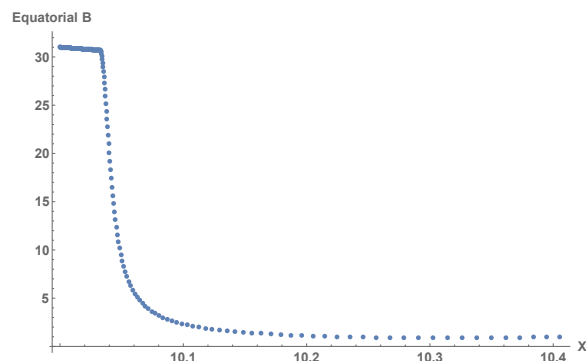


Figure 7. A plot of magnetic field strength along the equatorial plane in 2A. Note the deep minimum in  $B$  (0.874 nT).

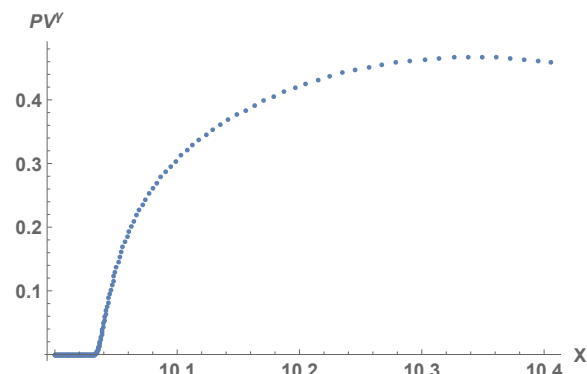


Figure 8. A plot of  $PV^\gamma$  along the equatorial plane in 2A.

Now consider case B, where a jump in  $PV^\gamma$  occurs on already stretched field lines, which corresponds to an arc embedded in the plasma sheet (where quiet evening arcs and growth phase

Modeling Sharp Jumps in Flux Tube Entropy in the Earth's Magnetosphere arcs are generated). In 1B, the field lines' shape is not drastically altered, but increased spacing between field lines and a decline in equatorial magnetic field from 8 nT to 3.13 nT are indicative of the jump's stretching effects on the field lines. Additionally, a sharp increase in an otherwise downward trending pressure (from 1.53561 nPa to 1.55473 nPa) is observed. Figures 9-12 show the results for case 1B.

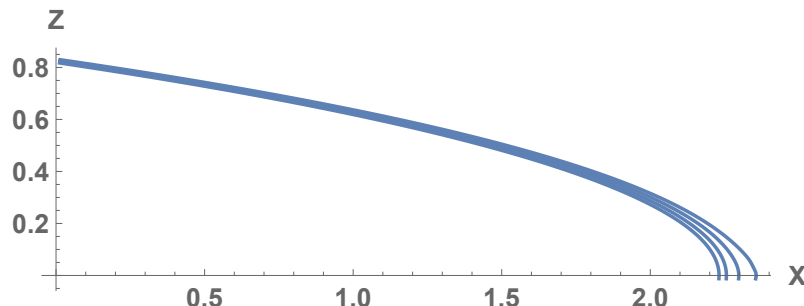


Figure 9. A plot of 4 field lines in 1B, with the field lines shown spaced equally in  $A$  ( $0.198 \text{ nT R}_E$ ). Note the increased spacing between the field lines.

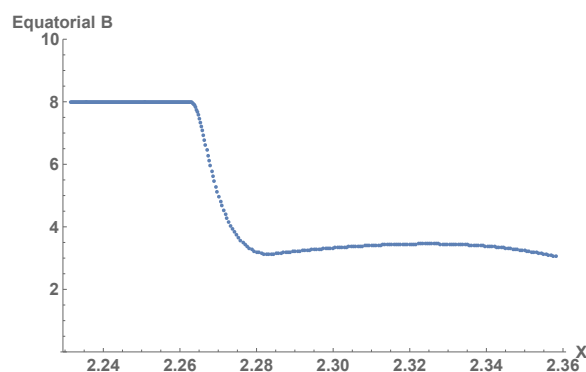


Figure 10. A plot of magnetic field strength along the equatorial plane in 1B.

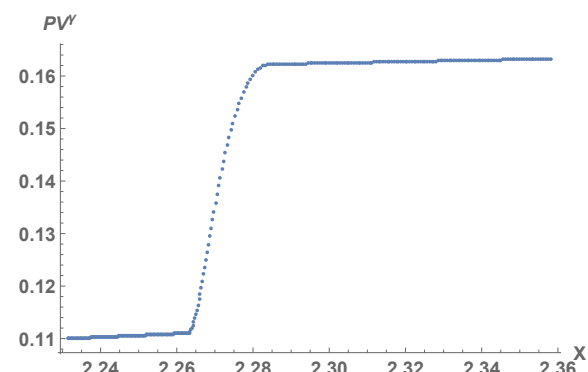


Figure 11. A plot of  $PV^\gamma$  along the equatorial plane in 1B.

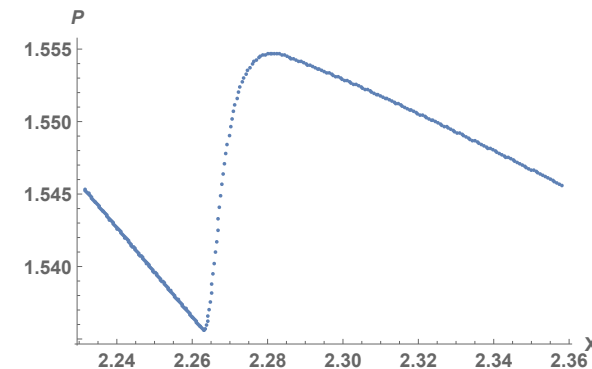


Figure 12. A plot of pressure along the equatorial plane in 1B.

The jump in 2B shows more noticeable effects (Figures 13-16). A knob forms in this scenario, and the equatorial magnetic field strength decreased to a deep minimum of 1.307 nT

Modeling Sharp Jumps in Flux Tube Entropy in the Earth's Magnetosphere from a starting point of 8 nT, indicating a sharp decline in equatorial field strength with increasing geocentric distance. The pressure meanwhile experiences a sharp increase in the middle of a decreasing trend (from 1.53658 nPa to 1.55882 nPa).

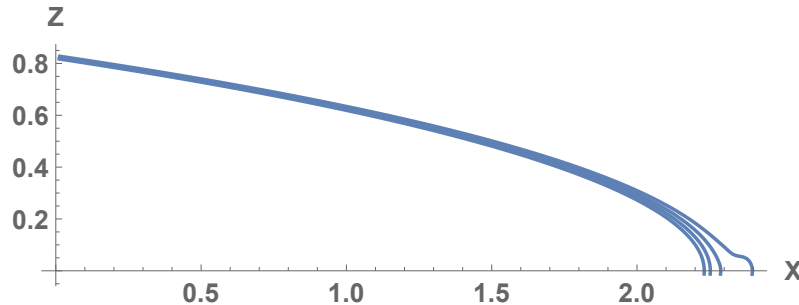


Figure 13. A plot of 4 field lines in 2B, with the field lines shown spaced equally in  $A$  ( $0.166 \text{ nT } R_E$ ). Note the increased spacing and formation of a knob.

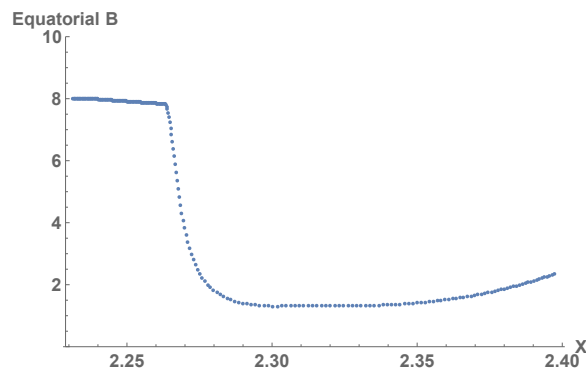


Figure 14. A plot of magnetic field strength along the equatorial plane in 2B. Note the deep minimum in  $B$  (1.307 nT).

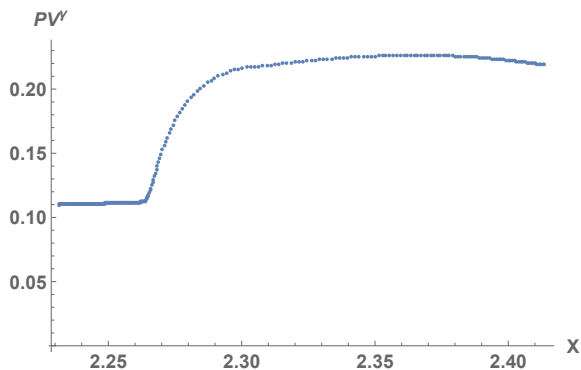


Figure 15. A plot of  $PV^\gamma$  along the equatorial plane in 2B.

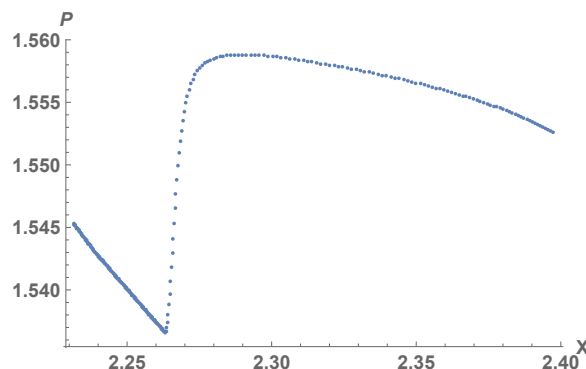


Figure 16. A plot of pressure along the equatorial plane in 2B.

One interesting immediate application of these results relates to the magnetospheric structure of a quiet evening auroral arc, an area of uncertainty that has long puzzled physicists.

The results in case B suggest the idea that one arc signature in the plasma sheet is a sharp decline in magnetic field with increasing geocentric distance. They also suggest that another prominent signature is the sharp increase in pressure along the equatorial plane as the jump takes place.

## Accuracy

The mathematical instability encountered in the study derives from the fact that this method involves no right-hand boundary condition. Consider the simple special case where (7) reduces to  $\nabla^2 A = 0$ , for which solutions have the form  $A = \sin(kz - \phi)[a(k)e^{kx} + b(k)e^{-kx}]$ . With no tailward boundary condition, the exponentially growing solution cannot be suppressed. As a result, a small-amplitude irregularity at small  $x$  grows exponentially to a large-amplitude irregularity at large  $x$ . The growth rate of the instability in  $x$  increases as the wavelength of the irregularity decreases. The shortest wavelength that can be represented is twice the spacing between two points along a field line. Thus, increasing the spacing between points slows down the growth of the instability, but it also reduces effective grid resolution and accuracy.

During the research, two test scenarios were used to check the validity and accuracy of the model. For the purposes of this report, these tests are referred to as test 1 and test 2. The former refers to a zero-pressure configuration with rounded field lines and was based on (11). The second test constitutes a more stretched configuration with nonzero pressure and was based on (12). These tests differ from the experimental scenarios in that no jump in  $PV^\gamma$  is instituted; thus, the shape of the field lines does not change with increasing  $A$ , and the model's general accuracy can be checked by comparing the shape of field lines tailward of the model's boundary of  $A = a_1$  to contours of constant  $A$  generated by (11) or (12). Since these cases are not very

Modeling Sharp Jumps in Flux Tube Entropy in the Earth's Magnetosphere  
volatile, the model computes accurate field lines over a range of  $10 \text{ nT } R_E$  in  $A$  for test 1 and 3  
 $\text{nT } R_E$  for test 2, much farther than needed to show the experimental scenarios' results.

For the experimental scenarios, an analytic expression only describes the first field line, after which the jump is initiated. Thus, other methods of checking accuracy were applied. First was a check of the field lines' conformity to the magnetospheric force balance equation given in (15), which describes the balance of particle pressure with magnetic pressure. The  $\nabla_{\perp}$  takes the

perpendicular component of the gradient of the total pressure ( $P + \frac{B^2}{2\mu_0}$ ).

$$\nabla_{\perp} \left( P + \frac{B^2}{2\mu_0} \right) = \kappa \frac{B^2}{\mu_0} \quad (15)$$

First, the computations from the unstructured grid of field lines were translated onto a dense rectangular grid through interpolation of the values of  $A$  and  $P$  over the  $xz$ -domain of the field lines to functions with respect to  $x$  and  $z$  in MATLAB. This step made it easier to calculate derivatives numerically through difference equations. Next, at each point in the rectangular grid, the gradient of pressure and the magnetic force, which should be equivalent in cases of total force balance, were computed. Of course, numerical error is present in all numerical studies, and the two were not expected to be exactly equal, but the intent of the grid testing was to determine the general level of force imbalance by comparing the two sides of (15) through contour plots.

These contour plots showed that the overall trends in the gradient of pressure and the magnetic force were generally similar; however, the specific details conveyed by the plots varied. For example, the differences between case 2A's contour plots (Figures 17 and 18) result from three effects: (1) actual inaccuracy in the numerical solutions; (2) error due to interpolation onto the rectangular grid and then taking first and second derivatives; (3) artifacts of the left and

Modeling Sharp Jumps in Flux Tube Entropy in the Earth's Magnetosphere  
upper-right boundaries of the calculation. The features in the upper right part of the plot do not  
follow the shape of the last field line computed (Figure 6) and are clearly boundary artifacts. The  
jagged structures in Figure 18 almost certainly represent errors in the interpolations and  
differentiations used for the grid testing. This test was not as effective as expected because it  
seems that most of the difference between Figures 17 and 18 came not from error in the model's  
calculations but from the grid testing itself. However, the contour plots' general similarity, when  
combined with an analysis of equatorial magnetic field shape, supports the accuracy of this  
study's conclusions.

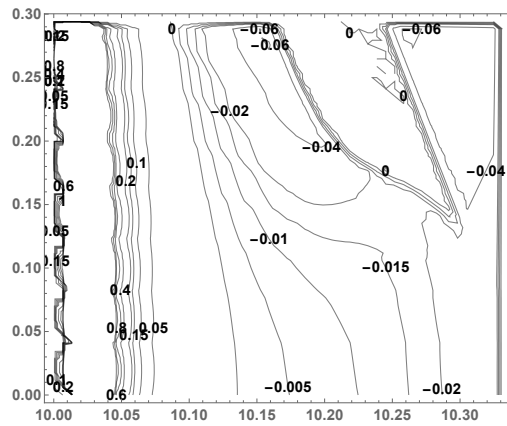


Figure 17. Gradient of pressure, x-component

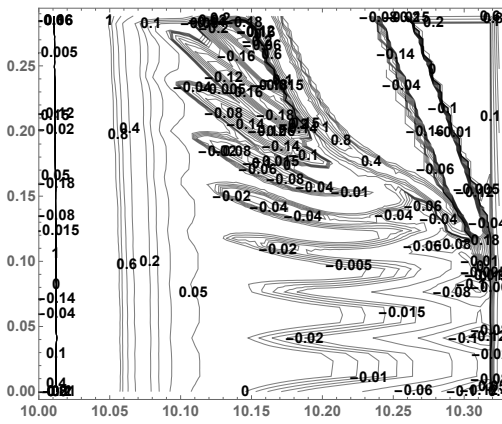


Figure 18. Magnetic force, x-component

The magnetic field shape test's logic proceeds as follows: a sharp jump in  $PV^\gamma$  entails a sharp jump in the pressure  $P$  when moving from field line to field line.  $P$  is constant along a field line in equilibrium, but the magnetic field along a field line is weakest at the equatorial plane, and hence, the effect of a jump in  $P$  on the gradual change of the magnetic field is greatest in magnitude at the equatorial plane. Figures 6 and 12 also show that the curvature of the field lines near the equatorial plane increases outward through the pressure increase. That increase in equatorial curvature  $\kappa$  can be calculated analytically if the jump is sharp enough that the total pressure is approximately conserved through the pressure increase. The approximate equation is:

$$\frac{\partial \kappa}{\partial A} = \frac{\kappa^2 B_<^2}{B^3} \left( 1 - \frac{B^2}{B_<^2} \right) \quad (16)$$

where  $B_<$  is the equatorial field strength before the jump. Constancy of total pressure is only a good approximation if the radius of curvature ( $1/\kappa$ ) is much larger than the thickness of the jump, so it only works a small distance through the jump. Results of this test (Figure 19) verify that the model is treating the base of the protuberance—the most critical region—accurately.

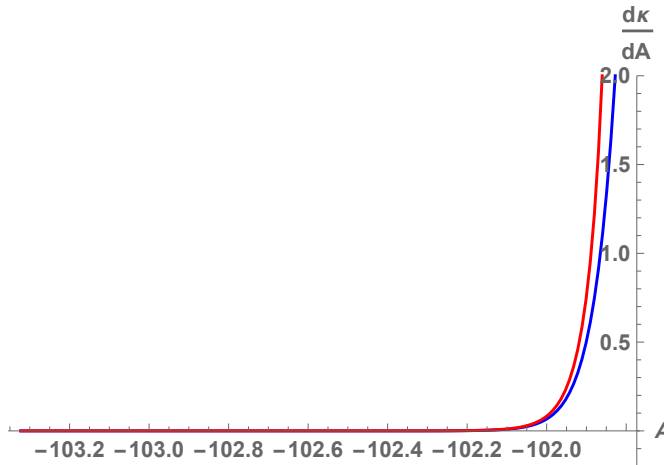


Figure 19. 2A analysis of magnetic field shape test. The blue line is the left-hand side of (16); the red line is the right-hand side. Note that the two sides of (16) accurately match up early on in the calculation.

## Conclusion & Future Directions

Ultimately, this study answered several questions regarding the structure of auroral arcs through an open-ended model that can accommodate magnetospheric configurations with sharp jumps in  $PV^\gamma$ . The model was able to compute the magnetic field for configurations with a range of values for  $\Delta PV^\gamma$  and  $A_w$ . Using this model to better comprehend plasma sheet properties could lead to better understanding of the substorm and auroral arcs' link to plasma sheet behavior.

Case A (non-arc-forming jump in  $PV^\gamma$ ) has led to significant conclusions. It showed that a sharp jump in  $PV^\gamma$  at the inner edge of the plasma sheet entails the creation of a region of very

Modeling Sharp Jumps in Flux Tube Entropy in the Earth's Magnetosphere  
weak magnetic field for the case of an ideal-MHD plasma sheet, where  $PV^Y$  jumps sharply from  
near zero to a middle plasma sheet value. Case 2A constitutes quite an exciting experiment, as it  
represents a solution to a longstanding computational problem in plasma sheet physics. Most  
models have failed to converge when trying to compute an equilibrium with a sharp edge; the  
sharpest inner edges computed so far have thicknesses of a few  $R_E$  [Hau *et al.*, 1989; Hau, 1991].  
This model has already improved this extent by an order of magnitude, allowing computations of  
thin jumps with  $A_w$  values as low as 1 nT  $R_E$ .

Meanwhile, in case B (arc-forming jump in  $PV^Y$ ), the model implies two signatures, a  
sharp decrease in equatorial magnetic field strength and a sharp increase in pressure along the  
equatorial plane. Hence, the model has produced significant findings on the magnetospheric  
structure that translates to a quiet evening arc in the ionosphere.

This study suffered from the mathematical instability mentioned in the “Accuracy”  
section above. In order to eliminate this limitation on the extent of the model, similar  
experiments will be implemented with a tailward boundary condition put in place to avoid  
exponentially spiraling error. If such a model succeeds in producing more accurate results, it will  
serve as an even more powerful tool than the model discussed in this study.

Of course, this study’s computer-simulation experiments are very open-ended, for they  
open up several exciting research areas. For example, future studies will explore the shape of the  
knob in case 2B and its consistency with physical conditions such as force balance. How much  
can the shape alter, and what role does the knob and its magnetic signature play in any  
magnetospheric or auroral phenomena, such as the onset of the expansion phase of the substorm?

### Modeling Sharp Jumps in Flux Tube Entropy in the Earth's Magnetosphere

In addition, this study's conclusions regarding the link between auroral arc formation and a jump in  $PV^\gamma$  can be tested against spacecraft data. A proposed NASA study looks at data from the Cluster Mission, THEMIS mission, and the recently launched Magnetospheric Multiscale Mission, each of which involves spacecraft flying in formation in the magnetosphere, to search for the magnetic signatures that this model predicts. If these signatures are found to be consistent with ground all-sky-camera observations, the quiet auroral arc will be successfully associated with particular plasma sheet behavior, an idea that scientists have been trying to demonstrate for nearly 50 years and a breakthrough in magnetospheric physics.

In order to account for a greater diversity of jumps in  $PV^\gamma$ , more experimental cases are being implemented through the model. These scenarios will vary in terms of not only  $\Delta PV^\gamma$  and  $A_w$  but also the stretching of the magnetic field. For example, consider the two cases 1D and 2D below, which belong to a family of cases with a more stretched magnetic field than that of family B. 1D has a  $\Delta PV^\gamma$  value of 0.0834 nPa  $(R_E/nT)^\gamma$  while 2D has a  $\Delta PV^\gamma$  value of 0.181437 nPa  $(R_E/nT)^\gamma$ . Each has an  $A_w$  value of 0.25 nT  $R_E$ . In 1D, a knob does not form, but a sharp drop in equatorial field strength from 19.472 nT to 7.90 nT is observed. The pressure undergoes a sharp increase from 0.150777 nPa to 0.276021 nPa. Figures 20-23 show the results for 1D.

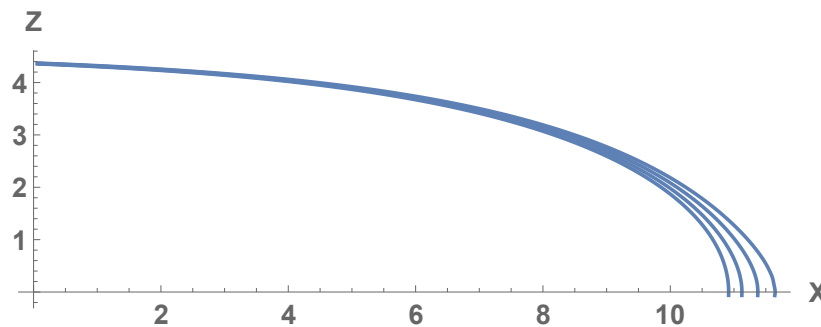


Figure 20. A plot of 4 field lines in 1D, with the field lines shown spaced equally in  $A$  ( $1.87032 \text{ nT } R_E$ ). Note the increased spacing between the field lines.

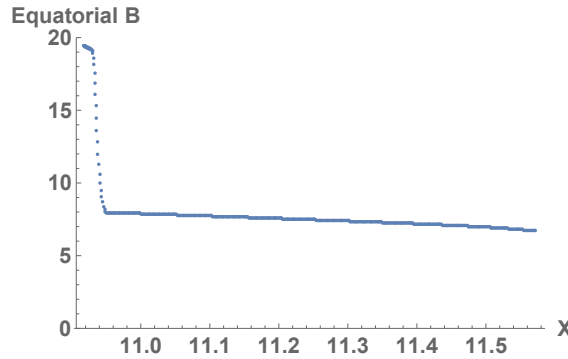


Figure 21. A plot of magnetic field strength along the equatorial plane in 1D.

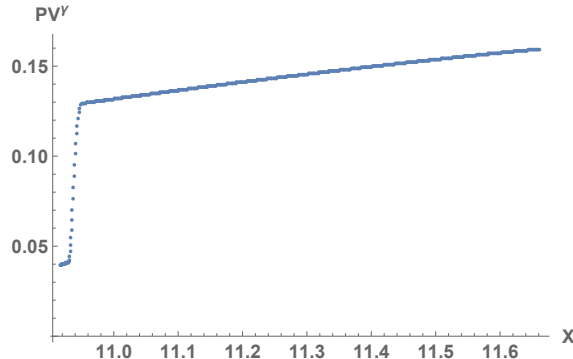


Figure 22. A plot of  $PV^\gamma$  along the equatorial plane in 1D.

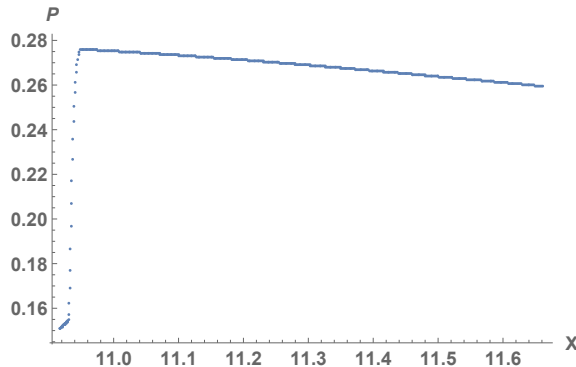


Figure 23. A plot of pressure along the equatorial plane in 1D.

Similar to 2B, case 2D displays much more prominent signatures of the jump in  $PV^\gamma$  (Figures 24-27). Knob formation takes place, and equatorial magnetic field strength experiences a sharp decline from 19.472 nT to 2.88 nT. The pressure experiences a sharp increase from 0.150777 nPa to 0.302397 nPa.

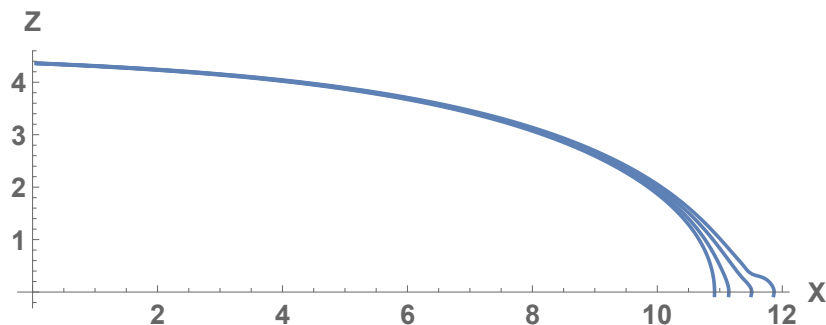


Figure 24. A plot of 4 field lines in 2D, with the field lines shown spaced equally in  $A$  (1.0264 nT  $R_E$ ). Note the increased spacing between the field lines and formation of a knob.

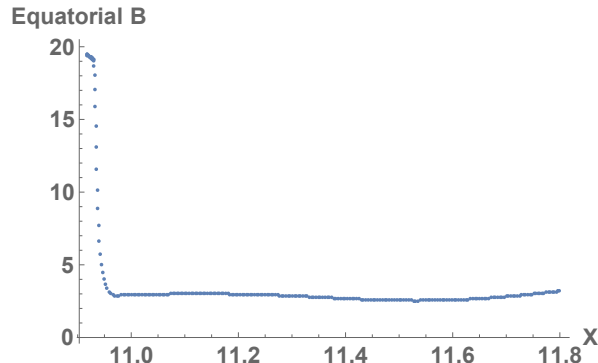


Figure 25. A plot of magnetic field strength along the equatorial plane in 2D.

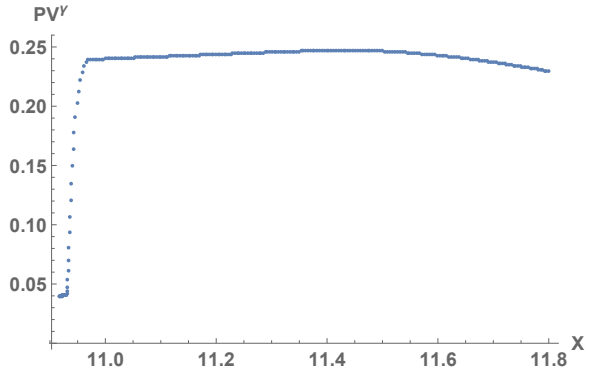


Figure 26. A plot of  $PV^Y$  along the equatorial plane in 2D.

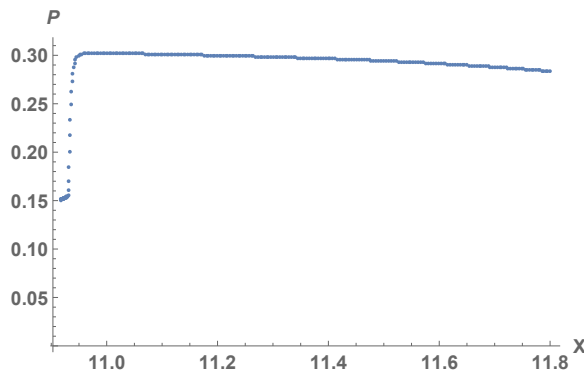


Figure 27. A plot of pressure along the equatorial plane in 2D.

Moreover,  $PV^Y$  cannot be easily measured along a given field line at a given time since calculating  $V$  involves measurement of  $B$ , which varies all along the field line. One future direction is to use the aforementioned spacecraft to search for jumps in  $PV^Y$  indirectly by analyzing data for the kind of magnetic field behavior predicted by this model. Also, the type of field lines in 2A that had a knob may exhibit a type of physical instability called a ballooning instability. Observational evidence exists for ballooning instabilities during the substorm [Roux *et al.*, 1991]. As a potentially direct link to plasma sheet structure during a substorm, 2A will be investigated through thorough tests of the magnetic field configuration for ballooning instability.

## References

- Baumjohann, W., and R. A. Treumann (1996), *Basic Space Plasma Physics*, Imperial College Press, London.
- Birn, J., and M. Hesse (1991), The substorm current wedge and field-aligned currents in MHD simulations of magnetotail reconnection, *J. Geophys. Res.*, 96, 1611-1618.
- Borovsky, J. E. (1993), Auroral arc thicknesses as predicted by various theories, *J. Geophys. Res.*, 98(A4), 6101-6138.
- Dendy, R. (Ed.) (1993), *Plasma Physics: An Introductory Course*, Cambridge University Press, Cambridge, UK.
- Fuchs, K., and G.-H. Voigt (1979), Self-consistent theory of a magnetospheric B-field model, in Quantitative modeling of magnetospheric processes, edited by W. P. Olson, p. 86, Am. Geophys. Un., Washington, D. C.
- Griffiths, D. J. (1981). *Introduction to Electrodynamics*, Prentice-Hall, Englewood Cliffs, New Jersey.
- Hau, L.-N., R. A. Wolf, G.-H. Voigt, and C. C. Wu (1989), Steady state magnetic field configurations for the Earth's magnetotail, *J. Geophys. Res.*, 94, 1303-1316.
- Hau, L.-N. (1991), Effect of steady-state adiabatic convection on the configuration of the near-Earth plasma sheet, 2, *J. Geophys. Res.*, 96(A4), 5591-5596.
- Lanzerotti, L. J. (2001), Space Weather Effects on Technologies, in *Space Weather, Geophysical Monograph Series Volume 125*, edited by P. Song, H. J. Singer and G. L. Siscoe, pp. 11-22, Am. Geophys. Un., Washington, D. C.
- Phillips, Tony (2014), "Near Miss: The Solar Superstorm of July 2012." NASA Science.
- Pritchett, P. L., and F. V. Coroniti (2011), Plasma sheet disruption by interchange-generated flow intrusions, *Geophys. Res. Lett.*, 38, doi:L10102, doi: 10.1029/2011GL047527.
- Raeder, J., P. Zhu, Y. Ge, and G. Siscoe (2010), OpenGGCM simulation of a substorm: Axial tail instability and ballooning mode preceding substorm onset, *J. Geophys. Res.*, 115, doi:A00I16, doi:10.1029/2010JA015876.
- Roux, A., S. Perraut, P. Robert, A. Morane, A. Pedersen, A. Korth, G. Kremser, B. Aparicio, D. Rodgers, and R. Pellinen (1991), Plasma sheet instability related to the westward traveling surge, *J. Geophys. Res.*, 96(A10), 17697-17714.
- Singh, A.K., and B.S. Bhaduria (2009), Finite difference formulae for unequal sub-intervals using Lagrange's interpolation formula, *Int. Journal of Math Analysis*, 3, 815-827.
- Sitnov, M. I., and M. Swisdak (2011), Onset of collisionless reconnection in two-dimensional current sheets and formation of dipolarization fronts, *J. Geophys. Res. (in press)*, doi:doi: 10.1029/2011JA016920.
- Vasyliunas, V. M. (1970), Mathematical models of magnetospheric convection and its coupling to the ionosphere, in *Particles and Fields in the Magnetosphere*, edited by B. M. McCormac, pp. 60-71, D. Reidel, Hingham, MA, Hingham, MA.

Suresh, A.  
Space Science

Modeling Sharp Jumps in Flux Tube Entropy in the Earth's Magnetosphere

Wolf, R. A. (2015), Physics of the Magnetosphere, unpublished manuscript.

Xing, X., and R. A. Wolf (2007), Criterion for interchange instability in a plasma connected to a conducting ionosphere, *J. Geophys. Res.*, 112, A12209, doi: 10.1029/2007JA012535.

## Annotated Bibliography

Baumjohann, W., and R. A. Treumann (1996), *Basic Space Plasma Physics*, Imperial College Press, London.

Baumjohann and Treumann's book covers the fundamentals of the expansive subject that is plasma physics. The authors focus on plasmas encountered naturally in space and discuss the physical, electrical, and magnetic properties of plasmas. They also discuss the basic theories underlying plasma physics. Much of the background information contained in this research paper was learned from reading the *Basic Space Plasma Physics* textbook.

Birn, J., and M. Hesse (1991), The substorm current wedge and field-aligned currents in MHD simulations of magnetotail reconnection, *J. Geophys. Res.*, 96, 1611-1618.

Birn and Hesse's article in the *Journal of Geophysical Research* presents a 3D simulation of the process of reconnection under conditions of ideal MHD. Though the simulation accurately displays plasma sheet dynamics during the substorm expansion phase, it does not have the ability to model especially sharp jumps in  $PV^Y$  due to its inability to account for small auroral arc widths.

Borovsky, J. E. (1993), Auroral arc thicknesses as predicted by various theories, *J. Geophys. Res.*, 98(A4), 6101-6138.

Borovsky's article in the *Journal of Geophysical Research* looks at 22 different proposed theories regarding auroral arcs and approximates auroral arc width in most of those cases. It concludes that the best general value for arc width in the case of most auroral arcs is between 100 m and 10 km based on scientists' observations of the thickness of ionospheric arcs and the conclusions of the different proposed theories.

Dendy, R. (Ed.) (1993), *Plasma Physics: An Introductory Course*, Cambridge University Press, Cambridge, UK.

This textbook covers the fundamentals of plasma physics in a general sense. It contains, therefore, not only the physics of naturally occurring plasmas in space but also that of man-made plasmas. The book also covers the applications of different plasmas and the numerical modeling methods used to study plasmas. This textbook provided this research paper with the equation of magnetic equilibrium.

Fuchs, K., and G.-H. Voigt (1979), Self-consistent theory of a magnetospheric B-field model, in Quantitative modeling of magnetospheric processes, edited by W. P. Olson, p. 86, Am. Geophys. Un., Washington, D. C.

This chapter in Fuchs and Vogit's book mostly discusses the lack of effective models of the Earth's magnetosphere that take into account the effect of the magnetic field on the behavior of plasma. This chapter was significant because it provided this paper with the form of the Grad-Shafranov partial differential equation found in the section entitled "The Method behind the Model."

Griffiths, D. J. (1981). *Introduction to Electrodynamics*, Prentice-Hall, Englewood Cliffs, New Jersey.

Griffiths' textbook covers vector calculus, electrostatics, electrodynamics,

Modeling Sharp Jumps in Flux Tube Entropy in the Earth's Magnetosphere  
magnetostatics, and magnetodynamics in a broad sense, delving into topics such as  
circuits and, of course, plasmas. For this paper, Griffiths' book provided the basic  
relationship between magnetic field and vector potential  $\mathbf{A}$  as well as the Maxwell  
equation for magnetic force and current in the magnetosphere.

Hau, L.-N., R. A. Wolf, G.-H. Voigt, and C. C. Wu (1989), Steady state magnetic field  
configurations for the Earth's magnetotail, *J. Geophys. Res.*, 94, 1303-1316.

This article in the Journal of Geophysical Research presents the modeling of a jump in  
 $PV^Y$  in a case with similar intents as case 2A. However, this ideal-MHD scenario cannot  
handle a particularly sharp jump in  $PV^Y$  and therefore is not very effective in computing  
an equilibrium with a sharp inner edge. The sharpness lacking in this scenario is what  
case 2A in this research paper attempts to include.

Hau, L.-N. (1991), Effect of steady-state adiabatic convection on the configuration of the near-  
Earth plasma sheet, 2, *J. Geophys. Res.*, 96(A4), 5591-5596.

This article is a continuation of the work described in the previous entry (Hau, L.-N., R.  
A. Wolf, G.-H. Voigt, and C. C. Wu (1989), Steady state magnetic field configurations  
for the Earth's magnetotail, *J. Geophys. Res.*, 94, 1303-1316.). The important novel  
contributions of this article are some new ideal-MHD scenarios with similar intents as  
those scenarios in the 1989 article but with more stretched magnetic field configurations.  
Again, the sharpness lacking in these scenarios is the property that case 2A tries to  
incorporate.

Lanzerotti, L. J. (2001), Space Weather Effects on Technologies, in *Space Weather, Geophysical  
Monograph Series Volume 125*, edited by P. Song, H. J. Singer and G. L. Siscoe, pp. 11-  
22, Am. Geophys. Un., Washington, D. C.

This chapter in Lanzerotti's book involves introductory information regarding space  
weather, scientific understanding of space weather during and since the Space Age, and  
the effect of space weather on technology such as satellites. This research paper  
employed information regarding substorms' effects on satellites from Lanzerotti's book.

Phillips, Tony (2014), "Near Miss: The Solar Superstorm of July 2012." NASA Science.

Phillips' article discusses the supermassive geomagnetic storm of 2012 that barely missed  
the Earth. It compares this storm to the supermassive Carrington event of 1859 and talks  
about the ramifications of such a phenomenon on technology on Earth. Its discussion of  
the effects of the substorms that accompany a supermassive geomagnetic storm on the  
power grid and telecommunications systems was taken into account in this research  
paper.

Pritchett, P. L., and F. V. Coroniti (2011), Plasma sheet disruption by interchange-generated flow  
intrusions, *Geophys. Res. Lett.*, 38, doi:L10102, doi: 10.1029/2011GL047527.

Similar to Birn and Hesse's article in the *Journal of Geophysical Research*, Pritchett and  
Coroniti's article in *Geophysical Research Letters* presents a 3D simulation of plasma  
behavior in the plasma sheet during substorm onset. Due to its inability to account for  
small arc widths, this simulation does not accurately model cases of sharp jumps in  $PV^Y$ .

Modeling Sharp Jumps in Flux Tube Entropy in the Earth's Magnetosphere

Raeder, J., P. Zhu, Y. Ge, and G. Siscoe (2010), OpenGGCM simulation of a substorm: Axial tail instability and ballooning mode preceding substorm onset, *J. Geophys. Res.*, 115, doi:A00I16, doi:10.1029/2010JA015876.

Just as Birn and Hesse's article in the *Journal of Geophysical Research* and Pritchett and Coroniti's article in *Geophysical Research Letters*, this article in the *Journal of Geophysical Research* presents a simulation of plasma behavior that fails to account for small arc widths and that therefore fails to accurately address cases of sharp jumps in  $PV^Y$ .

Roux, A., S. Perraut, P. Robert, A. Morane, A. Pedersen, A. Korth, G. Kremser, B. Aparicio, D. Rodgers, and R. Pellinen (1991), Plasma sheet instability related to the westward traveling surge, *J. Geophys. Res.*, 96(A10), 17697-17714.

This article in the *Journal of Geophysical Research* discusses data collected by a satellite and its implications. One such implication of the data is the potential connection between the substorm and ballooning instability, which this research paper briefly touches on.

Singh, A.K., and B.S. Bhaduria (2009), Finite difference formulae for unequal sub-intervals using Lagrange's interpolation formula, *Int. Journal of Math Analysis*, 3, 815-827.

Singh and Bhaduria's paper provides several computational formulas, including finite difference equations and methods for a variety of orders and situations. For example, the paper lists the formulas for three-point, four-point, and five-point finite difference equations with variable and constant spacing as well as with different centers of numerical differentiation. The five-point central difference equations with variable spacing were adapted to fit into this research paper's model.

Sitnov, M. I., and M. Swisdak (2011), Onset of collisionless reconnection in two-dimensional current sheets and formation of dipolarization fronts, *J. Geophys. Res. (in press)*, doi:doi:10.1029/2011JA016920.

Similar to Birn and Hesse's article in the *Journal of Geophysical Research*, Pritchett and Coroniti's article in *Geophysical Research Letters*, and the Raeder et al [2010] article in the *Journal of Geophysical Research*, this article in the *Journal of Geophysical Research* presents a 2D-simulation of plasma behavior in the plasma sheet during substorm onset. This model fails to account for small arc widths and therefore fails to accurately address cases of sharp jumps in  $PV^Y$ .

Vasyliunas, V. M. (1970), Mathematical models of magnetospheric convection and its coupling to the ionosphere, in Particles and Fields in the Magnetosphere, edited by B. M. McCormac, pp. 60-71, D. Reidel, Hingham, MA, Hingham, MA.

Vasyliunas's paper discusses past attempts to model the Earth's magnetosphere and then continues to express the qualitative attributes of those past models in more quantitative ways. One important result of this effort was his derivation of the Vasyliunas equation for the relationship between field-aligned electrical current and the gradient of  $PV^Y$ . This equation is included in this paper, and this paper's model is largely based off this equation.

Wolf, R. A. (2015), Physics of the Magnetosphere, unpublished manuscript.

Wolf's unpublished textbook contains basic background information regarding the

Modeling Sharp Jumps in Flux Tube Entropy in the Earth's Magnetosphere  
Earth's magnetosphere. It discusses in detail the structures and processes in the  
magnetosphere and provides a mix of quantitative and qualitative information. A cartoon  
image of the magnetosphere found in this textbook was included in this paper.

Xing, X., and R. A. Wolf (2007), Criterion for interchange instability in a plasma connected to a  
conducting ionosphere, *J. Geophys. Res.*, 112, A12209, doi: 10.1029/2007JA012535.

Xing and Wolf's paper in the *Journal of Geophysical Research* applies different methods  
to find the average or general values of pressure, flux tube volume, and flux tube entropy  
throughout the plasma sheet. The paper also studies the trend in these variables moving  
tailward in the plasma sheet. Xing and Wolf's paper includes much quantitative  
observational evidence, including the average observed value of  $PV^Y$  in the middle  
plasma sheet. This value was highlighted and utilized in one experimental scenario in this  
research paper.